Green Chemical Technology

SCIEPublish

Communication

Synthesis, Characterization and Thermochemical Energy Storage Potential of Tetraamminecopper(II) Sulfate Monohydrate

Mirzeta Saletović [1], Filip Brleković [2], Katarina Mužina [2] and Stanislav Kurajica [2,*]

[1] Department of Chemisty, Faculty of Natural Science and Mathematics, University of Tuzla, 75000 Tuzla, Bosnia and Hezegovina; mirzeta.saletovic@untz.ba (M.S.)

[2] Faculty of Chemical Engineering and Technology, University of Zagreb, 10000 Zagreb, Croatia; fbrlekovi@fkit.unizh.hr (F.B.); kmuzina@fkit.unizg.hr (K.M.)

* Corresponding author. E-mail: stankok@fkit.unizg.hr (S.K.)

Received: 24 March 2026; Revised: 15 April 2026; Accepted: 28 April 2026; Available online: 12 May 2026

ABSTRACT: Tetraamminecopper(II) sulfate monohydrate, $[Cu(NH_3)_4]SO_4 \cdot H_2O$, can be used as a thermochemical energy storage material. When heated, $[Cu(NH_3)_4]SO_4 \cdot H_2O$ releases ammonia gas and water, leaving behind $CuSO_4$. When $CuSO_4$ is cooled and exposed to ammonia, the reverse reaction occurs, forming $[Cu(NH_3)_4]SO_4$ and releasing the stored heat. The reaction occurs at medium temperatures, can store a significant amount of thermal energy, and is highly reversible, allowing repeated cycles of heat storage and release without significant material degradation. This type of thermochemical energy storage can be used in various applications, particularly industrial waste heat recovery and solar thermal energy storage. In this study, tetraamminecopper(II) sulfate monohydrate was synthesized by chemical precipitation and thoroughly characterized via various techniques. Phase identification was performed by powder X-ray diffraction (PXRD) and Fourier transformed infrared spectroscopy (FTIR). The morphology of the sample was examined by scanning electron microscopy (SEM), and its chemical composition and elemental distribution were analyzed by energy-dispersive X-ray spectroscopy (EDS). Thermal properties were investigated via differential scanning calorimetry (DSC) and thermogravimetric analysis (TGA). UV-Vis diffuse reflectance spectroscopy of the solid sample revealed a broad absorption band characteristic of $[Cu(NH_3)_4]SO_4 \cdot H_2O$, consistent with its dark blue color. XRD and FTIR analyses confirmed that the obtained sample is $[Cu(NH_3)_4]SO_4 \cdot H_2O$. SEM investigation showed that the prepared material consists of agglomerated particles of varying sizes. The process of thermal decomposition of the examined tetraamine copper(II) sulfate monohydrate takes place in three steps below 350 °C, followed by two additional steps at higher temperatures. Thermochemical energy storage potential of the prepared material is assessed on the basis of operating temperature range (20–200 °C), water elimination during the initial cycle, and volume changes in the course of charging/discharging process, yielding volumetric energy storage density estimation of 382 $MJ \cdot m^{-3}$.

Keywords: Ammonia chemical storage; Tetraamminecopper(II) sulfate monohydrate; Thermal analysis; Volumetric energy storage density

1. Introduction

Thermal energy storage (TES) is a technology that enables the storage and subsequent release of heat. TES can be used to balance energy supply and demand by storing energy from renewable sources, since these sources are intermittent. In this way, TES enhances the reliability and resilience of energy systems, improves energy efficiency, and reduces energy costs and greenhouse-gas emissions [1]. TES systems are divided based on the way in which heat is stored and released: The simplest are based on sensible heat storage, where heat is stored by raising or lowering the temperature of a suitable liquid or solid medium, such as a molten metal salt or concrete. Slightly more complex systems use latent heat storage, where heat is stored by changing the phase (aggregate state) of a suitable material, most often by freezing-melting processes. The materials used in these systems are called phase change materials (PCM), e.g., paraffin wax. Finally, the most complex method is thermochemical heat storage (TCES), where heat is stored by breaking or forming chemical bonds in a reversible reaction. The materials used in those systems are called thermochemical materials (TCM) [2].

When compared to sensible and latent heat storage, TCM can yield the highest heat storage capacity without thermal losses during the storage period. This allows for long-term storage of large amounts of energy and is ideal for applications where heat needs to be stored over a long period of time. Ideal thermochemical materials for energy storage should have: high storage densities, high reaction rates, and complete cycling reversibility without material degradation, enabling long-term use [3].

Many transition metals can be covalently bonded to one or more ligands in the form of complexes. Most commonly, transition metals such as nickel, cobalt, copper, manganese, and iron are used and paired with ligands like ammonia or water [4]. Numerous studies have shown that transition metal ammines are suitable for TCM. Currently, nickel chloride complex with ammonia, $Ni(NH_3)_6Cl_2$, offers the highest energy storage density [5]. However, although $NiCl_2$ has the highest density, it is prone to degradation, whereas $CuSO_4$ is often preferred for long-term cycling because it shows no material degradation after multiple cycles [6]. The reaction of $CuSO_4$ and NH_3, which forms $[Cu(NH_3)_4]SO_4$, is highly exothermic, with a heat release of 1.77 $MJ \cdot kg^{-1}$, which corresponds to an energy storage density of 6.38 $GJ \cdot m^{-3}$ [7]. In this case, the cycle consists of an endothermic process of decomposition of $[Cu(NH_3)_4]SO_4$, driven by generated excess thermal energy, and an exothermic complexation reaction between $CuSO_4$ and NH_3 at lower temperatures, whereby $[Cu(NH_3)_4]SO_4$ is formed again [7]. It is a promising material for medium-temperature thermal energy storage, particularly in applications where reversible reactions and medium-temperature ranges are needed. Disadvantages that currently prevent the commercial application of this process include cycle stability issues, low reaction rate, and material investment costs. Using pure sulfate salt as a storage material during the reaction with NH_3 results in a significant expansion of the material, which would require additional free volume in order to avoid significant mechanical stress [7].

In this research, $[Cu(NH_3)_4]SO_4 \cdot H_2O$ was prepared by the reaction of $CuSO_4 \cdot 5H_2O$ and NH_3 in an aqueous solution. The prepared complex was analyzed by UV-Vis, XRD, FTIR, SEM, and DSC/TGA. Finally, the thermochemical energy storage potential of the prepared material is assessed. Unlike previous reports, we considered the implementation of low operating temperatures, along with packing density and safety margins, thereby obtaining a more realistic estimate of volumetric energy storage density.

2. Materials and Methods

2.1. Synthesis

The following chemicals were used: copper(II) sulfate pentahydrate (p.a., Centrohem, Stara Pazova, Serbia), ammonia (25%, p.a., GRAM-MOL, Zagreb, Croatia), and ethanol (96%, MB Impeks d.o.o., Banja Luka, Bosnia and Herzegovina). Crystalline copper(II) sulfate was first crushed into a fine powder in a porcelain mortar. 10 g of powder was then transferred to a glass, and 10 mL of distilled water was added,

followed by 20 mL of concentrated ammonia solution with constant manual stirring using a glass rod. By the end of ammonia addition (~1 min), a clear azure-blue solution was obtained. Then, 50 mL of 96% ethanol was poured into an Erlenmeyer flask, and a glass tube was placed in the flask so that its end reached the bottom. Using the tube, 10 mL of distilled water was slowly added to the very bottom of the flask. After that, without moving the flask, the ammonia solution of copper(II) sulfate was introduced into the flask in the same way as the water, so that the layers of the blue solution and the colorless ethanol did not mix. After three days at room temperature, acicular dark blue crystals of tetraammine copper(II) sulfate monohydrate precipitated. The crystals were filtered using a Büchner funnel connected to a vacuum pump and washed first with 10 mL of ethanol to which three drops of ammonia had been added, and then with 20 mL of pure ethanol. The resulting product was dried at room temperature between sheets of filter paper (Figure 1a) without heating to avoid decomposition, and then stored in a tightly closed container to prevent the gradual loss of water and ammonia during air exposure.

(**a**) (**b**)

Figure 1. Photography of (**a**) synthesized $[Cu(NH_3)_4]SO_4 \cdot H_2O$ sample, (**b**) $[Cu(NH_3)_4]SO_4 \cdot H_2O$ sample heated to 500 °C.

2.2. Characterization

Diffuse reflectance spectroscopy (DRS) was performed using Ocean Insight QE Pro High-Performance spectrometer (Ocean Optics, Orlando, FL, USA) equipped with an integrating sphere. Reflectance spectra were measured in the range of 200–900 nm using $BaSO_4$ as a white standard.

Phase identification was performed by X-ray powder diffraction (XRD) analysis using a Rigaku Miniflex 600 diffractometer (Rigaku, Tokyo, Japan) with CuKα radiation. Data were collected in the 2θ range of 10° to 70°, with a step size of 0.01° and a scan speed of $10° \cdot min^{-1}$.

FTIR analysis was conducted on a Bruker Vertex 70 spectrometer (Bruker Optics, Karlsruhe, Germany) in attenuated total reflectance (ATR) mode, using samples pressed onto a diamond crystal. Spectra were recorded in the range of 400–4000 cm^{-1} with a resolution of 2 cm^{-1}, and the final spectrum represents the average of 32 scans.

The morphology of the samples was examined using Tescan Vega III Easyprobe scanning electron microscope (Tescan, Brno, Czech Republic) equipped with a tungsten filament, operating at an accelerating voltage of 10 kV. Samples were mounted on holders using self-adhesive carbon tape and sputter-coated with a gold-palladium alloy using Quorum SC 7620 sputter coater (Quorum Technologies, Laughton, UK).

Thermogravimetric analysis (DTA) was carried out using a NETZSCH STA 409 thermal analyzer (NETZSCH, Selb, Germany). Approximately 50 mg of the sample was placed in an α-Al_2O_3 crucible, which was also used as the reference material. The sample was heated from room temperature to 650 °C at a rate of 10 °C·min^{-1} under an air flow of 30 cm^3·min^{-1}.

Differential scanning calorimetry (DSC) was performed on LINSEIS DSC PT 1600 instrument (LINSEIS, Selb, Germany) under the same conditions: approximately 50 mg of the sample was placed in an α-Al_2O_3 crucible, heated from room temperature to 650 °C at 10 °C·min^{-1} in an air flow. The baseline was obtained by running an analysis with an empty crucible and was subtracted from the sample curve. To determine the energy for the process of interest, the peaks were integrated using a linear baseline.

3. Results

In Figure 2a, the UV-Vis spectrum of the synthesized sample is shown. As can be observed, the prepared complex shows a broad reflection band centered in the blue part of the visible spectrum. In the $[Cu(NH_3)_4]SO_4·H_2O$ complex, the Cu^{2+} ion is coordinated by four ammonia molecules, whereas the water molecule is not directly bound to copper; instead, it is hydrogen-bonded to the sulphate anion. Due to the dsp^2 hybridization of the copper(II) ion, the complex has a square planar geometry. The electrons of the central metal atom are under the influence of the static electric field of the ligands. This influence is the strongest on the d electrons, so the d orbitals of copper(II) are split into different energy levels. The energy difference between levels is such that the photon can excite an electron from a lower to a higher energy d orbital within the same d subshell (d-d transition). In this particular case, the d-d transition absorbs visible light in roughly red region and thus the complex assumes the complementary blue color [8].

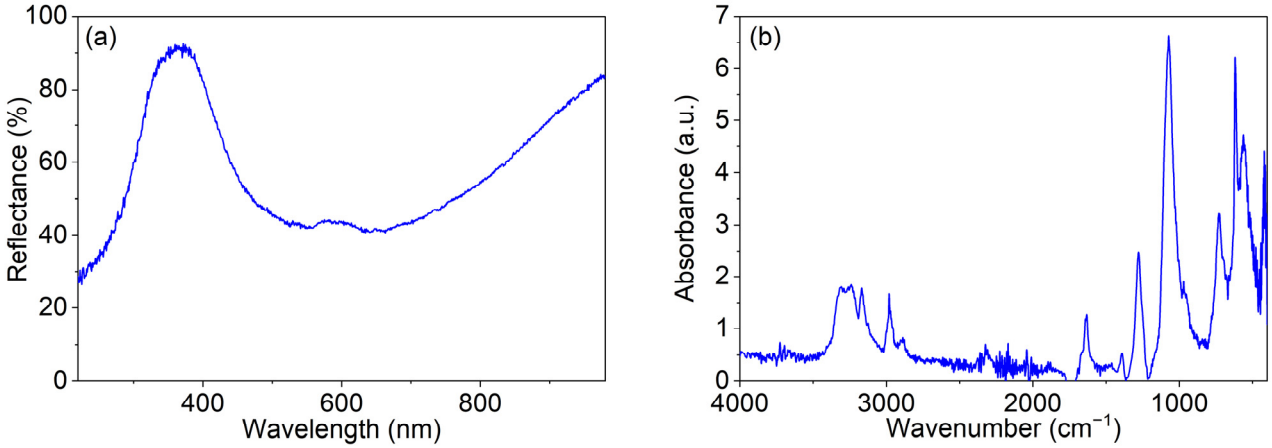

Figure 2. (**a**) UV-Vis spectrum of the synthesized sample, (**b**) FTIR spectrum of the synthesized sample.

The FTIR spectrum of the prepared sample is presented in Figure 2b. The absorption bands in the region 3400–3000 cm^{-1} are assigned to asymmetric and symmetric NH_3 stretching [9–11]. In this region, bands due to water O–H stretching also appear. Bands at 1635 and 1280 cm^{-1} are assigned to asymmetric and symmetric H–N–H bending vibrations, respectively, while the band at and 725 cm^{-1} is due to the rocking vibrations of the NH_3 molecule [9,10,12]. The band at 1635 cm^{-1} is also overlapped with the bending motion of the H_2O molecule. The absorption band at 1070 cm^{-1} is attributed to the stretching vibrations of the SO_4^{2-} anion. Additionally, the bending vibration of the sulfate anion appears at 625 cm^{-1} [10,11]. Finally, the band at 425 cm^{-1} is due to the Cu–N stretching vibration [10,11].

The micrographs of the prepared sample are shown in Figure 3. As can be seen, the prepared complex forms irregular particles of various shapes and sizes. The particles are agglomerated, creating secondary formations. For TCM performance, it is important how efficiently the ligand can move into and out of the

crystal lattice [13], which is dictated by the surface area and porosity [13]. However, to perform such measurements, degassing is required; since $[Cu(NH_3)_4]SO_4 \cdot H_2O$ is unstable, it undergoes decomposition, as the stability of the complex is governed by a gas–solid equilibrium that is highly sensitive to the partial pressure of ammonia. This precludes direct measurement of the specific surface area and pore size distribution. Based on the morphology shown in Figure 3, it could be argued that the relatively small crystals provide sufficient reaction sites, enabling fast charging/discharging rates and short diffusion paths (*i.e.*, the distance a gas molecule must travel through the solid product layer). However, the crystal morphology is likely to change during cycling.

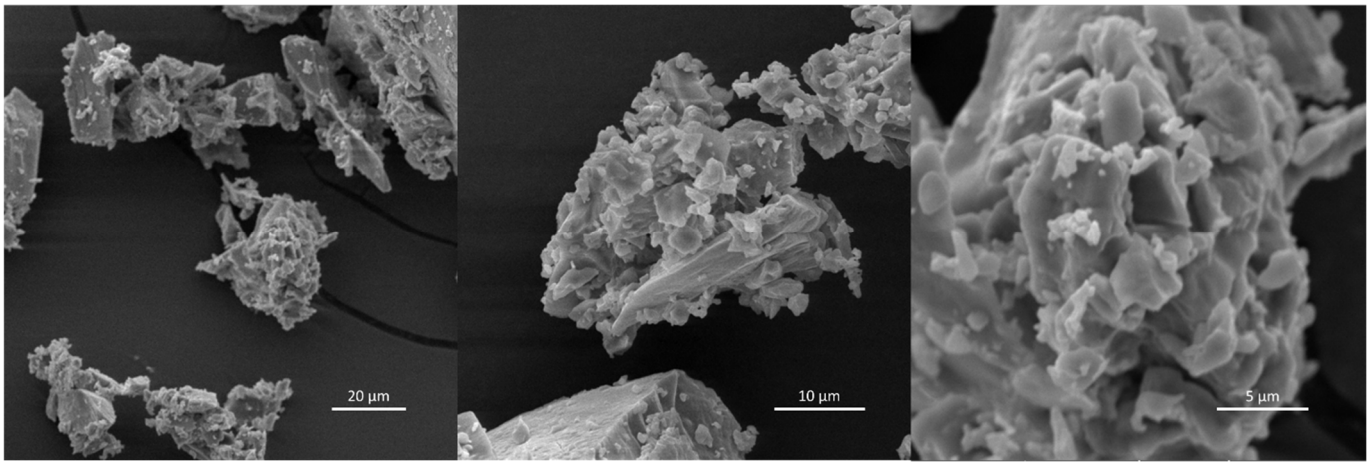

Figure 3. SEM micrographs of the synthesized sample.

The PXRD pattern of the prepared sample is given in Figure 4. The diffraction peaks are consistent with the ICDD PDF #73-762, so it can be concluded that $[Cu(NH_3)_4]SO_4 \cdot H_2O$ was successfully prepared. No other crystal phases were observed. The high intensity and narrow peaks point out to large crystals, which is in concordance with SEM micrographs (Figure 3).

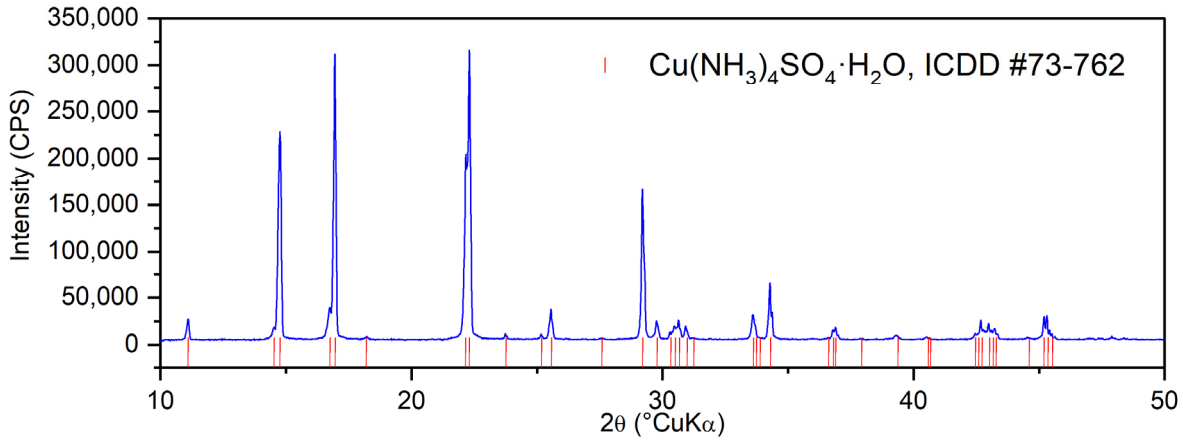

Figure 4. PXRD pattern of the synthesized sample.

Five stages of mass loss are clearly discernible on the TG curve (Figure 5). By deriving the TG curve, it is observed that the first stage consists of at least two processes, bringing the total number of mass loss stages to six. A similar observation can be made from the DSC curve (Figure 5), showing six large endothermic peaks, although two additional small endotherms could be observed. The temperatures corresponding to the peaks of the large endotherms are: 144, 172, 278, 350, 702, and 772 °C. According to literature, the endothermic peaks at 144 and 172 °C, and the corresponding mass loss could be attributed to

the loss of two ammonia molecules and one water molecule [14,15]. The mass loss measured from the TG curve yields 20.97%, which is in fair concordance with the theoretical mass loss of 21.20%. This is followed by the loss of the two remaining ammonia molecules at 278 and 350 °C [14,15]. Here, the measured mass loss for both processes yields 14.15%, while the theoretical loss equals 13.86%. Up to the temperature of 500 °C, the crystal color turns pale greenish, while the original complex morphology is retained (Figure 1b), although the crystals become very soft and easily collapse into powder. The mass loss is accompanied by two peaks at 278 and 350 °C, which, together with a small peak at 248 °C, could be attributed to the loss of two ammonia molecules. The following endotherms at 702 and 772 °C are due to the decomposition of $CuSO_4$ [14,15]. First, tetraamminecopper(II) sulfate monohydrate is decomposed to transient copper oxysulfate, $CuO{\cdot}CuSO_4$, releasing SO_2 and 1/2 O_2. Then, $CuO{\cdot}CuSO_4$ decomposes to CuO, SO_2 and 1/2 O_2. The combined mass loss due to these two decomposition processes is 32.65%, while the theoretical mass loss is 32.58%, which could be rated as excellent agreement. The mass fraction of the residual is 32.23%, while the theoretical fraction of CuO is 32.36%, which is again an excellent agreement. Unfortunately, a small DSC peak at 575 °C, which is not accompanied by mass los, could not be attributed to a particular process.

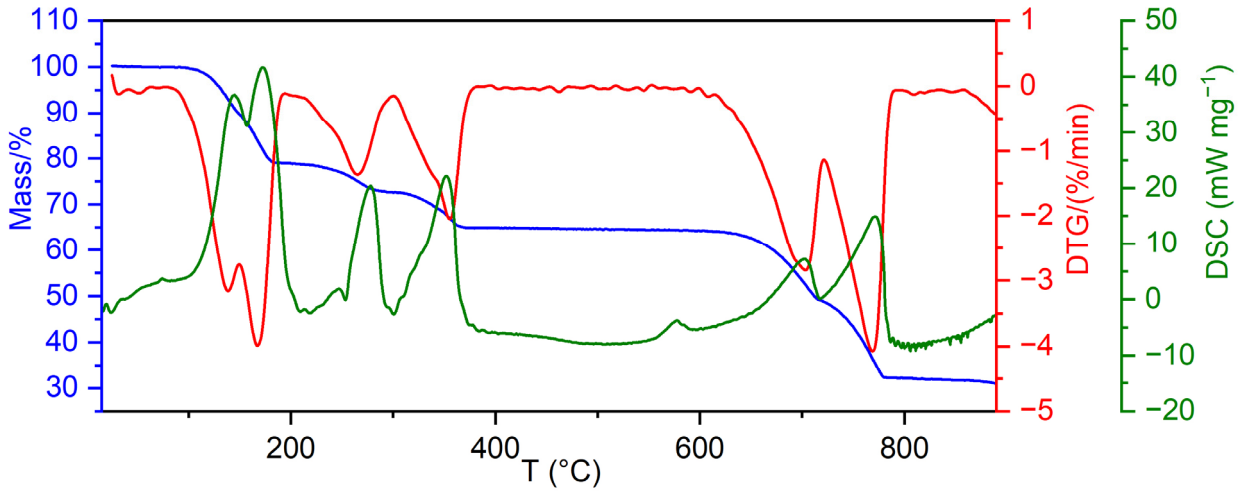

Figure 5. TG, DTG, and DSC curves of the synthesized sample.

4. Discussion

In an attempt to assess the thermochemical energy storage potential of the prepared material, the first step is to decide on the type of reactor and operating temperature range. The use of a static fixed-bed reactor is implied due to its simplicity, since there are no moving parts, and good solid-fluid contact is ensured. The choice of temperature range is primarily influenced by the available heat source. The vast majority of industrial waste heat output falls below the temperature of 200 °C [16], while flat plate and evacuated tube solar heat collectors also have thermal output below 200 °C [17]. Additionally, process equipment for thermochemical energy storage is generally simpler and more cost-effective at low temperatures. An additional benefit of operating at low temperatures is the prevention of irreversible decomposition of the sulfate backbone, thus ensuring full reversibility. Since the temperature of heat release and the heat released depend on the ammonia pressure, employing low pressure in the system can facilitate the discharging of the material (release of heat by reaction with ammonia and water vapor) at room temperature or slightly above it. Therefore, it seems reasonable to choose a temperature range between 20 and 200 °C.

According to DSC and TGA curves (Figure 5) and literature [14,15], in this temperature range, the charging phase consists of $[Cu(NH_3)_4]SO_4{\cdot}H_2O$, endothermic loss of one water and two ammonia molecules. Integration of two overlapped peaks in the 20 to 200 °C region (Figure 5) gives an energy of

approximately 156 $kJ \cdot mol^{-1}$. However, before calculating volumetric energy storage density, one should consider that although dehydration is an endothermic reaction and thus stores heat, in most cases water is driven off and removed during the first cycle, so it does not participate in subsequent cycles. Also, if water is not removed, it can form ammonia hydroxide and cause corrosion, both of which are highly undesirable. Therefore, since the water molecule does not participate in reversible cycles, the energy used for its removal is lost, and the storage mechanism will be the reversible reaction between anhydrous copper(II) sulfate and ammonia gas.

This does not mean that hydrate should not be used. The use of hydrate complex offers several practical and economic advantages: First of all, hydrated salts are widely available and affordable in comparison to anhydrous ones, and their usage as the initial material makes the storage system more cost effective. Due to less hygroscopicity, hydrates are more stable and easier to handle since because intense absorption of water leading to clumping is avoided. Once the first cycle is complete and the water is removed, the material's energy storage performance, reversibility, and cycle stability are identical to those of a system that started with anhydrous salt [18].

Thus, the endothermic effect should be corrected for the loss of a water molecule, which contributes about 56 $kJ \cdot mol^{-1}$ to the total energy effect [19], resulting in a usable endothermic effect of approximately 100 $kJ \cdot mol^{-1}$. Based on the latter, as well as the molar mass of 227.73 $g \cdot mol^{-1}$ and the volumetric density of 1810 $kg \cdot m^{-3}$ [4], the volumetric energy storage density of $[Cu(NH_3)_4]SO_4$ in the temperature range between 20 and 200 °C can be estimated to be approximately 795 $MJ \cdot m^{-3}$. For comparison, paraffin wax, which is often used as a heat storage material, has volumetric energy storage density, primarily derived from its latent heat of fusion, between 146 and 210 $MJ \cdot m^{-3}$ [20].

Additionally, when calculating for a fixed-bed reactor, a packing factor of 0.6–0.7 must be applied to account for the air gaps between the granules [21]. Thus, assuming the packaging factor of 0.6, the volumetric energy storage density is reduced to approximately 477 $MJ \cdot m^{-3}$. Reactors used are designed to store the gasses in a separate tank to avoid an extreme rise of pressure during charging [22]. Additionally, there is no need to consider volume changes since the calculation was done for teraamminecopper(II) sulphate, which decomposes during charging to diamminecopper(II) sulfate, accompanied by mass loss and volume contraction [4]. The changes due to thermal expansion of the material can also be neglected. However, in the dimensioning of a fixed-bed reactor, the required volume should be multiplied by an additional safety factor of at least 1.25 to ensure safety and functionality under non-ideal conditions. With this correction, the volumetric energy storage density is reduced to approximately 382 $MJ \cdot m^{-3}$, which is still significantly better than paraffin wax. The volumetric energy storage densities that refer to real conditions are generally difficult to compare because studies are not standardized. The reactors, operating temperature range, cycles, porosity, carrier, composites, dopants, etc., differ a lot across studies. For example, a recent study [23] presents an investigation of sol-gel derived CaO-based composites with Al and Ce dopants added in order to reduce CaO sintering and enhance carbonation kinetics. A heat storage density of 1600 $kJ \cdot kg^{-1}$ after 50 cycles, assuming 80% conversion, was calculated. Thus, using the theoretical density of $CaCO_3$, the volumetric energy storage density is estimated to be 4.336 $GJ \cdot m^{-3}$. However, if powder or granules are assumed, this value would be significantly lower. Also, the temperature range for this process is commonly between 750 and 950 °C.

The $Cu(NH_3)_4SO_4/CuSO_4$ couple is noted for its excellent reversibility, enabling thousands of ammoniation/deammoniation cycles and fast response [6]. Some shortcomings of this system, like thermal expansion, gas management, and economics, have been addressed here. Others like high corrosivity of ammonia and low thermal conductivity could be mitigated by using stainless steel process equipment and metal foams. The kinetics of this couple is defined by rapid reaction rates, *i.e.*, fast charging and discharging [4], although constrained by solid-state diffusion at low temperatures [24].

5. Conclusions

Dark-blue solid tetraamminecopper(II) sulfate monohydrate, $[Cu(NH_3)_4]SO_4 \cdot H_2O$, was prepared by chemical precipitation. UV-Vis, PXRD, and FTIR analyses confirmed that the product of synthesis is $[Cu(NH_3)_4]SO_4 \cdot H_2O$, while SEM investigation revealed that the prepared material consists of agglomerated platelets of varying sizes. According to TG analysis, tetraamminecopper(II) sulfate monohydrate undergoes a series of six endothermic decomposition steps. On the basis of operating temperature range between 20 and 200 °C and volume changes in the course of charging/discharging processes, volumetric energy storage density of tetraamminecopper(II) sulfate monohydrate was estimated to be 382 $MJ \cdot m^{-3}$.

Acknowledgments

M.S. would like to gratefully acknowledge the hospitality of the Faculty of Chemical Engineering and Technology, University of Zagreb, Croatia. The aegis of the University of Zagreb is gratefully acknowledged by S.K. and K.M.

Author Contributions

Conceptualization, M.S. and S.K.; Methodology, M.S. and S.K.; Validation, F.B. and K.M.; Formal Analysis, M.S., F.B. and K.M.; Investigation, M.S., F.B., K.M. and S.K.; Resources, S.K.; Data Curation, S.K.; Writing—Original Draft Preparation, S.K.; Writing—Review & Editing, S.K. and K.M.; Visualization, S.K. and F.B.; Supervision, S.K.; Project Administration, S.K.; Funding Acquisition, S.K.

Ethics Statement

Not Applicable.

Informed Consent Statement

Not Applicable.

Data Availability Statement

The original contributions presented in this study are included in the article. Further inquiries can be directed to the corresponding author.

Funding

This research was conducted within the framework of the project HEMCAT, financed by the European Union's NextGenerationEU fund from source 581—The recovery and resilience mechanism in the framework of programme financing of public higher education institutions and public scientific institutes. The investigation is aided by the mobility project inside the CEEPUS network: SI-0708-12-2425 (Umbrella)—Chemistry and Chemical Engineering.

Declaration of Competing Interest

The authors declare that they have no known competing financial interests or personal relationships that could have appeared to influence the work reported in this paper.

References

1. Koohi-Fayegh S, Rosen MA. A review of energy storage types, applications and recent developments. *J. Energy Storage* **2020**, *27*, 101047. DOI:10.1016/j.est.2019.101047

2. Abedin AH, Rosen MR. A critical review of thermochemical energy storage systems. *Open Renew. Energy J.* **2011**, *4*, 42–46. DOI:10.2174/1876387101004010042
3. Deutsch M, Müller D, Aumeyr C, Jordan C, Gierl-Mayer C, Weinberger P, et al. Systematic search algorithm for potential thermochemical energy storage systems. *Appl. Energy* **2016**, *183*, 113–120. DOI:10.1016/j.apenergy.2016.08.142
4. Müller D, Knoll C, Gravogl G, Jordan C. Eitenberger E, Friedbacher G, et al. Medium temperature thermochemical energy storage with transition metal ammonias—A systematic material comparison. *Appl. Energy* **2021**, *285*, 116470. DOI:10.1016/j.apenergy.2021.116470
5. Wu S, Li TX, Wang RZ. Experimental identification and thermodynamic analysis of ammonia sorption equilibrium characteristics on halide salts. *Energy* **2018**, *161*, 955–962. DOI:10.1016/j.energy.2018.07.129
6. Liu H, Shen X, Guo Q, Sun H. A data-driven approach towards fast economic dispatch in electricity–gas coupled systems based on artificial neural network. *Appl. Energy* **2021**, *286*, 116480. DOI:10.1016/j.apenergy.2021.116480
7. Müller D, Knoll C, Gravogl G, Lager D, Welch JM, Eitenberger E, et. al. $CuSO_4$/$[Cu(NH_3)_4]SO_4$-Composite Thermochemical Energy Storage Materials. *Nanomaterials* **2020**, *10*, 2485. DOI:10.3390/nano10122485
8. Guspita D, Ulianas A. Optimization of complex NH_3 with Cu^{2+} ions to determine levels of ammonia by UV-Vis spectrophotometer. *J. Phys. Conf. Series* **2020**, *1481*, 012040. DOI:10.1088/1742-6596/1481/1/012040
9. Nakamoto K. Spectra of Inorganic and Coordination Compounds. In *Application in Coordination, Organometallic, and Bioinorganic Chemistry*, 6th ed.; John Willey & Sons: Hoboken, NJ, USA, 2009.
10. Mansournia M, Azizi A. A single precursor route to synthesize CuO and CuS nanostructures based on copper ammine and thiourea complexes. *J. Mater. Sci. Mater. Electron.* **2016**, *27*, 7908–7919. DOI:10.1007/s10854-016-4782-0
11. Bahrami-Rad S, Hajiboland R, Khatamian M. Foliar Application of Nano Tetraammine Copper (II) Sulfate Complex Influences Cu and Fe Homeostasis, Phenolics and Lignin Biosynthesis in Tobacco (Nicotiana rustica) Plants. *J. Sci IRI* **2022**, *33*, 105–116.
12. Garba HW, Abubakar K, Abdullahi MS, Watanpal R. Synthesis, Spectroscopy Study of Copper (II) Sulphate Pentahydrate, Tetra-Amminocopper (II) Sulphate and Bis-Ethylenediamine Copper (II) Sulphate in the Catalytic Reduction of Nitrophenol Derivatives. *Int. J. Sci. Eng. Sci.* **2020**, *4*, 19–26. Available online: https://www.academia.edu/download/92555708/95-IJSES-V4N9.pdf (accessed on 11 February 2026).
13. Chen X, Aziz M. Solid-gas thermochemical energy storage materials for renewable energy integration in power grids. *Energy Storage Mater.* **2025**, *80*, 104340. DOI:10.1016/j.ensm.2025.104340
14. Mathew S, Nair CGR. Thermal decomposition kinetics: Part XV. Kinetics and mechanism of thermal decomposition of tetraamine copper(II) sulphate monohydrate. *Thermochim. Acta* **1989**, *144*, 33–43. DOI:10.1016/0040-6031(89)85082-8
15. Živković ŽD. The kinetics and mechanism of the thermal decomposition of tetramminecopper(II) sulphate monohydrate. *Thermochim. Acta* **1992**, *203*, 251–257. DOI:10.1016/0040-6031(92)85200-F
16. Dadi D, Introna V, Benedetti M. Decarbonization of Heat through Low-Temperature Waste Heat Recovery: Proposal of a Tool for the Preliminary Evaluation of Technologies in the Industrial Sector. *Sustainability* **2022**, *14*, 12626. DOI:10.3390/su141912626
17. Ajarostaghi SSM, Mousavi SS. Solar energy conversion technologies: Principles and advancements. In *Solar Energy Advancements in Agriculture and Food Production Systems*; Gorjian S, Campana PE, Eds.; Academic Press: Cambridge, UK, 2022; pp. 29–76.
18. Schmieder L, Schaeffer C, Denner S, Wedl G, Smith J, Winter F. Stability of copper sulphate pentahydrate for thermochemical energy storage in a suspension reactor. *J. Energy Storage* **2026**, *144*, 119804. DOI:10.1016/j.est.2025.119804
19. Lide DR. *CRC Handbook on Chemistry and Physics*, 85th ed.; CRC Press: Boca Raton, FL, USA, 2004.
20. Patil BY, Pawar R, Suryawanshi H, Patil S, Salunkhe P. Optimizing thermal energy storage: A review of paraffin wax as phase change material and evacuated tube collector in solar energy storage. *Int. Res. J. Mod. Eng. Technol. Sci.* **2025**, *7*, 5272–5286. Available online: https://www.irjmets.com/upload_newfiles/irjmets71200169763/paper_file/irjmets71200169763.pdf (accessed on 11 February 2026).
21. Ye H, Tao YB, Wu ZH. Performance improvement of packed bed thermochemical heat storage by enhancing heat transfer and vapor transmission. *Appl. Energy* **2022**, *326*, 119946. DOI:10.1016/j.apenergy.2022.119946
22. Han XC, Xu HJ, Xu T, Zhao CY. Magnesium-based thermochemical reactor with multiporous structures for medium-temperature solar applications: Transient modelling of discharge capability. *Sol. Energy Mater. Sol. Cells* **2022**, *238*, 111630. DOI:10.1016/j.solmat.2022.111630

23. Zhu Z, Xu Q, Li X, Zhang S, Hai C, Zhou Y. Al–Ce Co-modified for enhanced long-cycle performance of $CaCO_3$-Based thermochemical energy storage materials. *Sol. Energy Mater. Sol. Cells* **2026**, *295*, 114020. DOI:10.1016/j.solmat.2025.114020
24. Gu T, Huš M, Araya SS, Likozar B, Gallucci F, Liso V. Thermocatalytic ammonia synthesis beyond conventional Haber-Bosch: Principles, advances, challenges and opportunities. *Prog. Energy Combust. Sci.* **2026**, *112*, 101262. DOI:10.1016/j.pecs.2025.101262